Conformational Transition Occurring upon Amyloid Aggregation of the HET-s Prion Protein of *Podospora anserina* Analyzed by Hydrogen/Deuterium Exchange and Mass Spectrometry†

Alexis Nazabal,*,‡ Suzana Dos Reis,§ Marc Bonneu,§ Sven J. Saupe,§ and Jean-Marie Schmitter‡

CNRS FRE 2247 Institut Européen de Chimie et Biologie, 16, Avenue Pey Berland 33607 Pessac, France, and Laboratoire de Génétique Moléculaire des Champignons, Institut de Biochimie et Génétique Cellulaires, UMR 5095 CNRS Université Victor Segalen Bordeaux 2-1, Rue Camille Saint-Saëns, 33077 Bordeaux Cedex, France

Received March 17, 2003; Revised Manuscript Received May 28, 2003

ABSTRACT: The [Het-s] infectious element of the filamentous fungus *Podospora anserina* corresponds to the prion form of the HET-s protein. HET-s (289 amino acids in length) aggregates into amyloid fibers in vitro. Such fibers obtained in vitro are infectious, indicating that the [Het-s] prion can propagate as a self-perpetuating amyloid aggregate of the HET-s protein. Previous analyses have suggested that only a limited region of the HET-s protein is involved in amyloid formation and prion propagation. To document the conformational transition occurring upon amyloid aggregation of HET-s, we have developed a method involving hydrogen/deuterium exchange monitored by MALDI-MS. In a first step, a peptide mass fingerprint of the protein was obtained, leading to 87% coverage of the HET-s primary structure. Amyloid aggregates of HET-s were obtained, and H/D exchange was monitored on the soluble and on the amyloid form of HET-s. This study revealed that in the soluble form of HET-s, the C-terminal region (spanning from residues 240−289) displays a high solvent accessibility. In sharp contrast, solvent accessibility is drastically reduced in that region in the amyloid form. H/D exchange rates and levels in the N-terminal part of the protein (residues 1−220) are comparable in the soluble and the aggregated state. These results indicate that amyloid aggregation of HET-s involves a conformational transition of the C-terminal part of the protein from a mainly disordered to an aggregated state in which this region is highly protected from hydrogen exchange.

Prions are infectious proteins that are able to propagate an abnormal conformational state. In mammals, the prion form of the PrP protein is responsible for a class of fatal neurological diseases termed TSEs (transmissible spongiform encephalopathies) (*1*). Prion diseases in fact belong to a larger class of debilitating affections that are all characterized by the deposition of protein aggregates termed amyloids (*2*). Among these amyloid diseases are common age-related neurodegenerative disorders such as Alzheimer's and Parkinson's disease. Amyloids are fibrillar protein aggregates characterized by a cross-β structure and a high resistance to proteolysis (*3*). There is, however, a major difference between prion diseases and other amyloidoses since only prion diseases are transmissible. Prion proteins also exist in fungal microorganisms (yeast and the filamentous fungus *Podospora anserina*) (*4*). Propagation of these fungal prions is intimately connected with amyloid formation (*5*), indicating that yeast and fungal prion proteins can represent valuable model systems not only to analyze prion propagation but also the general process of amyloid formation.

The [Het-s] infectious element of the fungus *P. anserina* corresponds to the prion form of the HET-s protein (*6*). Strains expressing the HET-s protein exist under two states: a normal state termed [Het-s*], and a prion infected state termed [Het-s]. A [Het-s*] strain is converted to the prion infected state by simple contact with a [Het-s] strain (*7*). The [Het-s] prion is involved in a genetically controlled cell death reaction termed heterokaryon incompatibility. Namely, when the HET-s protein (in its prion state) is coexpressed with a variant of HET-s termed HET-S, a cell death reaction occurs. In other words, the [Het-s] prion is not detrimental per se but becomes lethal only when coexpressed with HET-S. HET-s and HET-S differ by 13 residues, and HET-S lacks the prion properties (*8*). In vivo, a HET-s-GFP fusion protein undergoes a transition from a soluble to an aggregated state upon transition to the prion state, thus suggesting that [Het-s] propagates as a self-perpetuating HET-s aggregate (*9*). Recombinant full-length HET-s forms amyloid aggregates in vitro (*10*). The transition from the soluble to the aggregated state is accompanied by an increase in β-sheet content. Biolistic introduction of aggregated recombinant HET-s protein into fungal cells induces emergence of the [Het-s] prion with a high frequency, thus demonstrating that prion infectivity can be created in vitro from recombinant protein in this system (*11*). The HET-s protein displays two domains, a N-terminal globular domain spanning residues 1−230, approximately, and a C-terminal region that is proposed to

† We gratefully acknowledge the financial support of CNRS and of the Région Aquitaine, including a grant for A.N. This work was supported in part by the GIS prion. S.D.R. is a recipient of a fellowship from the Ministère de la Recherche et de l'Enseignement supérieur.

* To whom correspondence should be addressed. E-mail: a.nazabal@iecb-polytechnique.u-bordeaux.fr.

‡ CNRS FRE 2247 Institut Européen de Chimie et Biologie.

§ UMR 5095 CNRS Université Victor Segalen Bordeaux 2-1.

10.1021/bi0344275 CCC: $25.00
Published on Web 07/02/2003

be poorly structured (*12*). This C-terminal domain of HET-s is essential for prion propagation in vivo and amyloid formation in vitro (*12*).

Mass spectrometric analysis of hydrogen/deuterium exchange (HXMS) is a powerful tool to probe protein structure and dynamics. The technique exploits the fact that hydrogen atoms involved in hydrogen bonds or buried in the core of the protein do not exchange readily with solvent deuterons. Rates of hydrogen exchange reflect solvent accessibility. Generally, high exchange rates are indicative of poor structure. Conversely, when the labile hydrogen atoms of a protein are involved in secondary structure or in noncovalent interactions, exchange rates are decreased (*13*, *14*). For a detailed characterization of solvent accessibility in specific regions, the protein can be submitted to proteolysis prior to HXMS analysis. H/D exchange is quenched by lowering both pH and temperature (pH 2, 0 °C). Under these conditions, short cleavage times can be obtained with immobilized pepsin, thus limiting back exchange during this step (*15*).

Amyloid aggregates are resistant to conventional methods of higher-order structure determination. One has therefore to rely on alternate methods to gain insight into the process of amyloid formation. Hydrogen exchange has been used to analyze the structural properties of several amyloid peptides. It was shown that amide protons in amyloid aggregates are highly resistant to hydrogen exchange (*16*−*18*). In the present work, the HET-s prion protein has been studied by HXMS, using matrix assisted laser desorption-ionization mass spectrometry (MALDI-MS). This methodology has been used to probe solvent accessibility for the soluble and amyloid form of the protein. The time-course incorporation of deuterium characterized along the sequence revealed that exchange rates are drastically reduced in the C-terminal region of the protein upon transition from the soluble to the amyloid state.

MATERIALS AND METHODS

HET-s Expression and Purification. The *het-s* open-reading frame was amplified by PCR from plasmid DNA using oligonucleotides s1 (5′-CT-CAAACTCATATGTCA-GAACCG-3′) and s2 (5′-ATAAGCTTAGTGATGATGGT-GATGGTGATTATCCCAGAACCC-3′), cloned into the *Nde*I and *Hind*III sites of the pET21a vector (Novagen) and introduced into BL21(DE3) pLysS cells. Cells were grown to 0.5 OD in 2× YT medium, and expression was induced by addition of 1 mM isopropyl *β*-D-thiogalactoside. After 4 h, cells were harvested by centrifugation, frozen at −80 °C, and lysed in 150 mM NaCl and 100 mM Tris-HCl, pH 8. The lysate was centrifuged for 20 min at 20 000*g*. The pellet was washed in the same buffer and resuspended in denaturing buffer (8 M guanidinium HCl, 150 mM NaCl, and 100 mM Tris-HCl, pH 8). The lysate was incubated with Talon Resin (Clontech) for 1 h at 20 °C, and the resin was washed with 8 M urea, 150 mM NaCl, and 100 mM Tris-HCl, pH 8. The HET-s protein was eluted from the resin in the same buffer containing 200 mM imidazole. For renaturation, dithiothreitol was added to 20 mM final concentration, and the sample was applied to a HiTrap desalting column (Amersham Biosciences) equilibrated with 150 mM NaCl, 100 mM Tris-HCl, pH 8, and 1 mM dithiothreitol. HET-s amyloids were obtained as previously described (*10*). In brief, soluble HET-s protein at 30 mM was inoculated with 3 mM preformed aggregates and incubated for 12 h at room temperature. Aggregates were recovered by centrifugation for 20 min at 10 000*g*.

Back Exchange Controls. A pepsin digest of HET-s was diluted 19:1 in D_2O and incubated for 2 h at 25 °C to achieve complete exchange of backbone amide protons for deuterium. After incubation, the exchange was quenched at 0 °C by addition of 0.1% trifluoroacetic acid (TFA, Pierce). After quenching, the peptide mixture was loaded on a C18 ZipTip (Millipore). The peptide fraction eluted from the ZipTip (the eluent was a 10 mg/mL solution of α-cyano-4-hydroxycinnamic acid (MALDI matrix) in 7:3 acetonitrile/ethanol (Mallinckrodt Baker) containing 0.1% TFA, kept at 0 °C) was directly spotted on the MALDI target under nitrogen flow. After drying, the sample was analyzed by MALDI-MS in the reflex mode. The relative back exchange (%) was determined for each peptide by comparing the maximal theoretical number of exchanged amide hydrogen atoms and the corresponding experimental value.

Hydrogen/Deuterium Exchange on Soluble HET-s Protein. HET-s protein (1 mL, 30 μM MQ H_2O) was centrifuged for 20 min at 10 000*g*. A total of 5 μL (30 μM) of the supernatant was diluted 1:20 in D_2O and incubated at 25 °C for variable times (from 5 to 120 min). After incubation, a 5 μL aliquot (7.5 pmol) of the labeled solution was treated under strong agitation with immobilized pepsin (10 μL, 45 units) at pH 2 and 0 °C (exchange quenching conditions). Digestion was followed by a short centrifugation (10 000*g*, 30 s), and a 5 μL aliquot of the supernatant containing the HET-s digest was submitted to C18 ZipTip purification by means of a gradient in three steps. The three fractions were eluted with 1 μL of a solution of 10 mg/mL α-cyano-4-hydroxycinnamic acid in 2:8:1; 4:6:1; 7:3:1 acetonitrile/ethanol/0.1% aqueous TFA, respectively, and were directly spotted on the target under nitrogen flow. After drying, the target was transferred as quickly as possible (less than 1 min) to the mass spectrometer. The time from sample spotting to data collection is kept constant for each sample analysis.

Hydrogen/Deuterium Exchange on HET-s Amyloid Fibrils. Aggregated HET-s (1 mL, 30 μM, H_2O MQ) was centrifuged for 20 min at 10 000*g*. The pellet was resuspended with 1 mL of H_2O MQ. A 5 μL aliquot (30 μM) of the aggregated solution was diluted 1:20 in D_2O and vortexed before incubation at 25 °C for variable times (between 5 and 120 min). After incubation, 5 μL of the labeled solution was treated under strong agitation in 4 M urea with immobilized pepsin (10 μL, 45 units) at pH 2 and 0 °C (exchange quenching conditions). After digestion, the sample was treated in the same way as the soluble form.

Microscopy. A fraction of the protein suspension (30 μM) used for exchange experiments on amyloid fibers was put onto a 400 mesh copper electron microscopy grid coated with a plastic film (Formvar). To avoid rapid desiccation, sedimentation was allowed during 10−30 min in a moist Petri dish. Grids were then rinsed with 15−20 drops of freshly prepared 2% uranyl acetate in water (passed over 0.22 μm Millipore filters), dried with filter paper, and observed with a Phillips Tecnai 12 Biowin electron microscope at 80 kV.

Data Analysis. The spectra were baseline corrected, and the number of deuterium atoms incorporated in a given

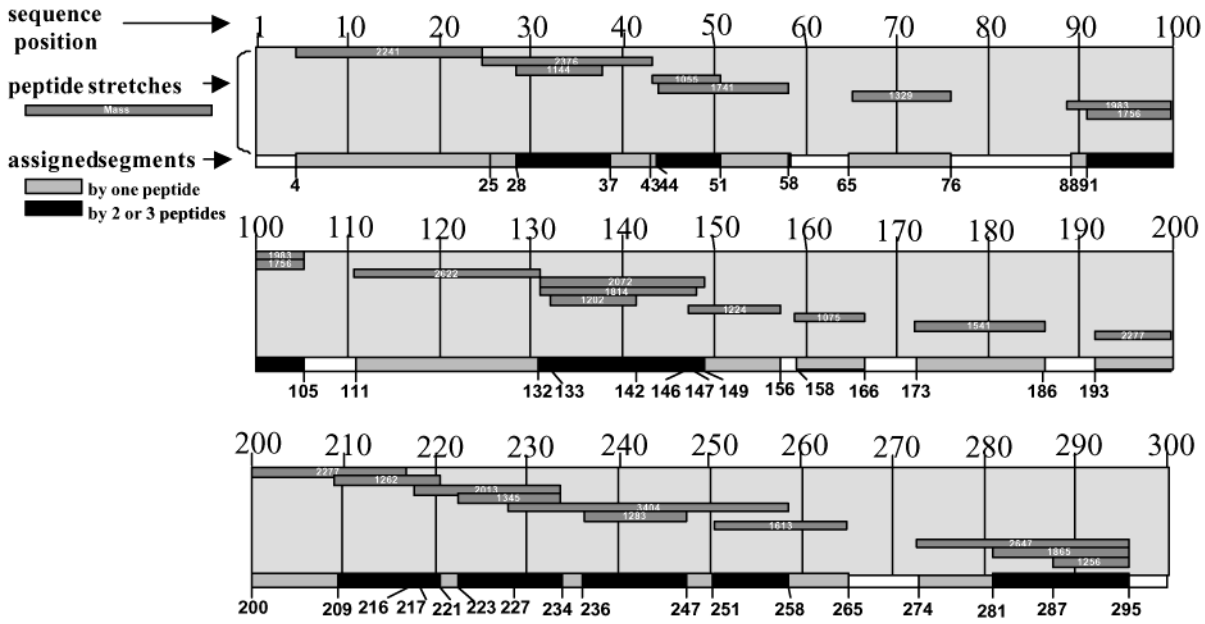

FIGURE 1: Sequence coverage of HET-s obtained by combined MALDI-MS, MALDI-PSD, and LC-MS/MS analysis of the peptide mixture obtained after pepsin digestion of nondeuterated HET-s.

Table 1: Peptide Mass Fingerprinting of HET-s Protein[a]

peptides analyzed by H/D exchange					
calculated mass[b]	observed mass[b]	position	sequence	ZipTip elution fraction[c]	method of identification[d]
1055.66	1055.65	43−51	RLDIAKAR	20% ACN	LC-MS/MS
1075.62	1075.64	158−166	KIVDQVARF	20% ACN	LC-MS/MS
1144.62	1144.63	28−37	VQLGRPFGRD	20% ACN	MALDI-PSD
1202.69	1202.69	133−142	VSRRQKQTSL	20% ACN	MALDI-PSD
1224.62	1224.60	146−156	TAWALYDGKSL	20% ACN	exact mass
1256.52	1256.48	287−295	WDNHHHHHH	20% ACN	exact mass
1262.60	1262.57	209−221	AAMSDAAAQKIDA	20% ACN	LC-MS/MS
1283.75	1283.71	236−247	RARVQLGNVVTA	20% ACN	LC-MS/MS
1329.65	1329.67	65−76	PRFHSSAPTDKS	20% ACN	exact mass
1345.71	1345.70	223−234	VGRNSAKDIRTE	20% ACN	LC-MS/MS
1403.58	1403.54	286−295	FWDNHHHHHH	20% ACN	exact mass
1541.85	1541.82	173−186	AFPIEAVCHKLAEI	20% ACN	exact mass
1613.78	1613.75	251−265	HGGIRISDQTTNSVE	20% ACN	exact mass
1741.98	1741.95	44−58	RLDIAKARLSRWGEA	20% ACN	LC-MS/MS
1756.92	1756.89	91−105	FESAQKTSKRYELVA	20% ACN	MALDI-PSD
1815.09	1814.06	132−147	LVSRRQKQTSLAKKTA	20% ACN	LC-MS/MS
1865.81	1865.77	281−295	YGGKGFWDNHHHHHH	20% ACN	LC-MS/MS
1983.09	1983.07	89−105	LLFESAQKTSKRYELVA	40% ACN	exact mass
2014.10	2014.08	217−234	QKIDAIVGRNSAKDIRTE	20% ACN	LC-MS/MS
2072.20	2072.16	132−149	LVSRRQKQTSLAKKTAWA	40% ACN	LC-MS/MS
2241.08	2241.10	4−25	PFGIVAGALNVAGLFNNCVDCF	20% ACN	LC-MS/MS
2277.09	2277.12	193−216	DEASLTILKDAAGGIDAAMSDAAA	40% ACN	LC-MS/MS
2376.15	2376.17	25−43	FEYVQLGRPFGRDYERCQL	40% ACN	LC-MS/MS
2622.43	2622.38	111−132	VVFEDKDMKPIGRALHRRLNDL	70% ACN	MALDI-PSD
2647.25	2647.31	274−295	RVLIGNEYGGKGFWDNHHHHHH	70% ACN	LC-MS/MS
3403.85	3403.79	227−258	SAKDIRTEERARVQLGNVVTAAALHGGIRISD	70% ACN	exact mass

[a] Peptide mass fingerprinting of the HET-s protein. The HET-s protein was digested with pepsin, and generated peptides were assigned using MALDI-MS exact mass matching, MALDI-MS-PSD, or LC-MS/MS. To limit as much as possible selective desorption phenomena associated with MALDI-MS, a microchromatographic gradient separation in three steps was applied using C18 ZipTips. [b] $[M + H]^+$ monoisotopic peaks. [c] Acetonitrile content in ZipTip eluent fraction. [d] Identification method. Exact mass indicates that only one peptide from HET-s matches the experimental mass within 20 ppm. Other peptides were identified using MALDI-PSD or Ion Trap LC-MS/MS.

peptide was determined from the centroid value of its isotopic peak cluster using the formula given in eq 1 (*19*)

$$D_{(t)} = \frac{m(t) - m(0)}{m(100) - m(0)} N \quad (1)$$

where $m(t)$ is the observed centroid mass of the peptide at time point t, $m(0)$ is the observed mass at time point 0 (for unlabeled peptides), $m(100)$ is the observed mass for a fully exchanged peptide (see back exchange control procedure), and N is the total number of peptide amide protons in the peptide.

Because in-exchange occurring during pepsin digestion is very limited for each peptide (less than 5% of deuterium

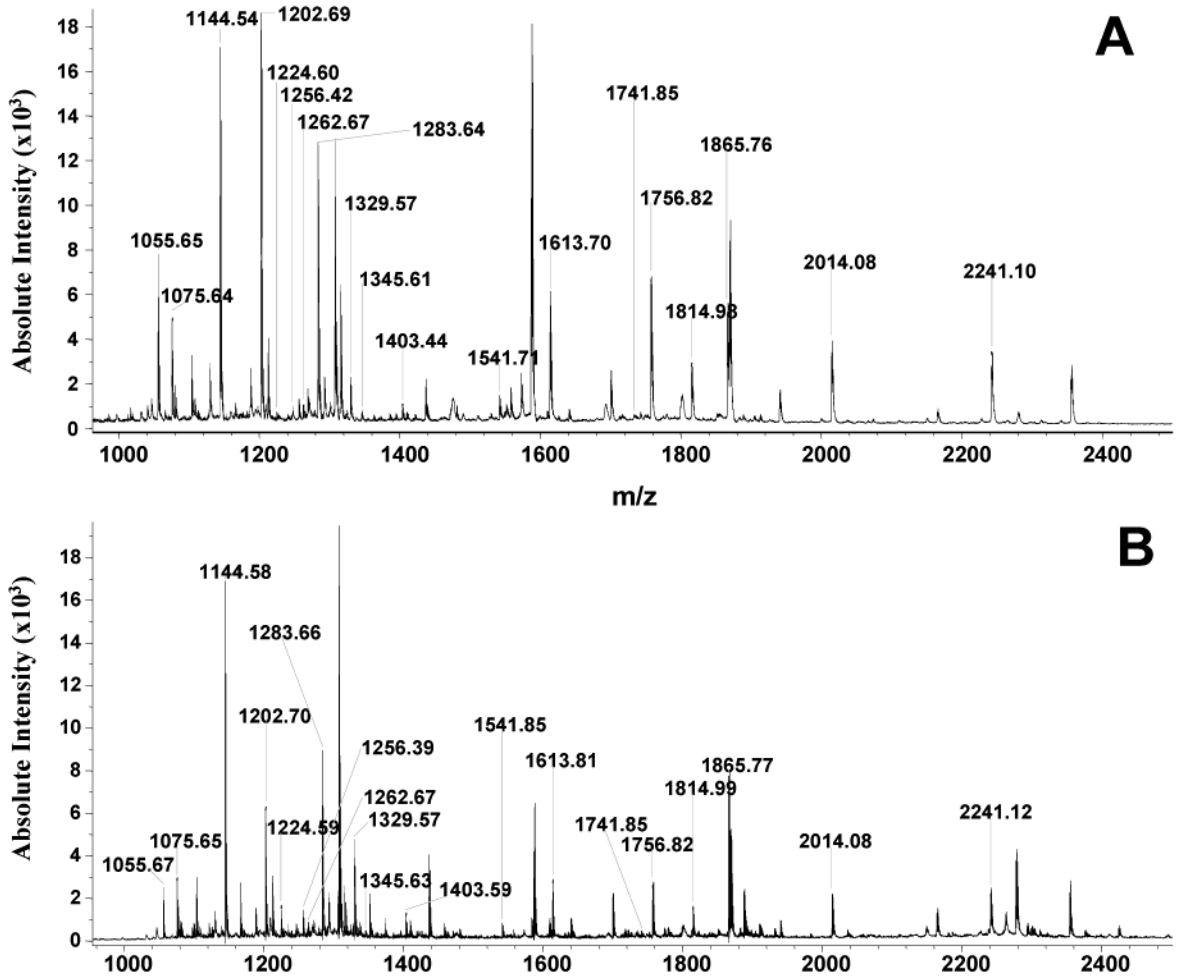

FIGURE 2: MALDI-MS analysis of the peptide mixture obtained after pepsin digestion of HET-s (nondeuterated) in soluble (A) and aggregated form (B). In both cases, the protein digest was submitted to C18 ZipTip simplification. The spectra presented correspond to the 20% acetonitrile elution step.

incorporation), we have chosen to consider $m(0)$ as the mass of unlabeled peptide observed for each peptide. When a large deuterium oxide concentration and a constant pH and temperature are maintained during exchange experiments, each amide hydrogen follows first-order kinetics. The exchange rate quantification leads to a more quantitative interpretation of the data and can be obtained from the following expression:

$$(1/N)P = e^{(-k_{ex}t)} \quad (2)$$

where P is the number of protected hydrogen atoms in the peptide, k_{ex} is the sum of each amide hydrogen exchange rate constant of the peptide, and t is the incubation time in D_2O.

From eq 2, it follows that populations of hydrogen atoms having different exchange rate constants can be distinguished in plots of ln[P] versus t. Exchange rates were calculated from logarithmic plots of the data. To characterize the solvent accessibility to deuterium oxide for peptides that have different total numbers of amide protons, we have calculated the percentage of deuterium incorporation ($\%D_{(t)}/N$). For the determination of deuterium incorporation into the HET-s primary sequence, we have chosen to consider the percentage of deuterium incorporation of an overlapping region as the average of the percentage of deuterium incorporation of all peptides involved in the overlapping region (Figure 1).

Mass Spectrometry. MALDI mass spectra were acquired on a Bruker Reflex III mass spectrometer equipped with a nitrogen laser with an emission wavelength of 337 nm. Spectra were obtained by accumulating an average of 100 shots in the positive ion mode, while the laser spot was manually scanned over a surface area of about 0.2 mm^2. Deflection of the low mass ions was used to enhance the target protein signal. Mass spectra of full-length HET-s were obtained in the linear mode (20 kV accelerating voltage). Mass spectra of HET-s digests were acquired in the reflectron mode, using an external calibration with a mixture of eight peptides covering a 900−3500 Da mass range. In this case, measured masses were monoisotopic $[M + H]^+$ ions. Mass values given in the text for exchange experiments correspond to m/z of the centroid of the envelope of the cluster for protonated molecular ions $[M + H]^+$. For post source decay analysis, the reflectron voltage was stepped down in 10−12 steps to record all fragment ions, including immonium ions. LC-MS/MS analysis of HET-s peptides was performed by means of an ion trap mass spectrometer operated in the electrospray mode (LCQ DecaXP, Thermo Finnigan) and interfaced to a Dionex-LC Packings chromatographic system (C18 column, 75 μm ID, 150 mm long). After analysis, the

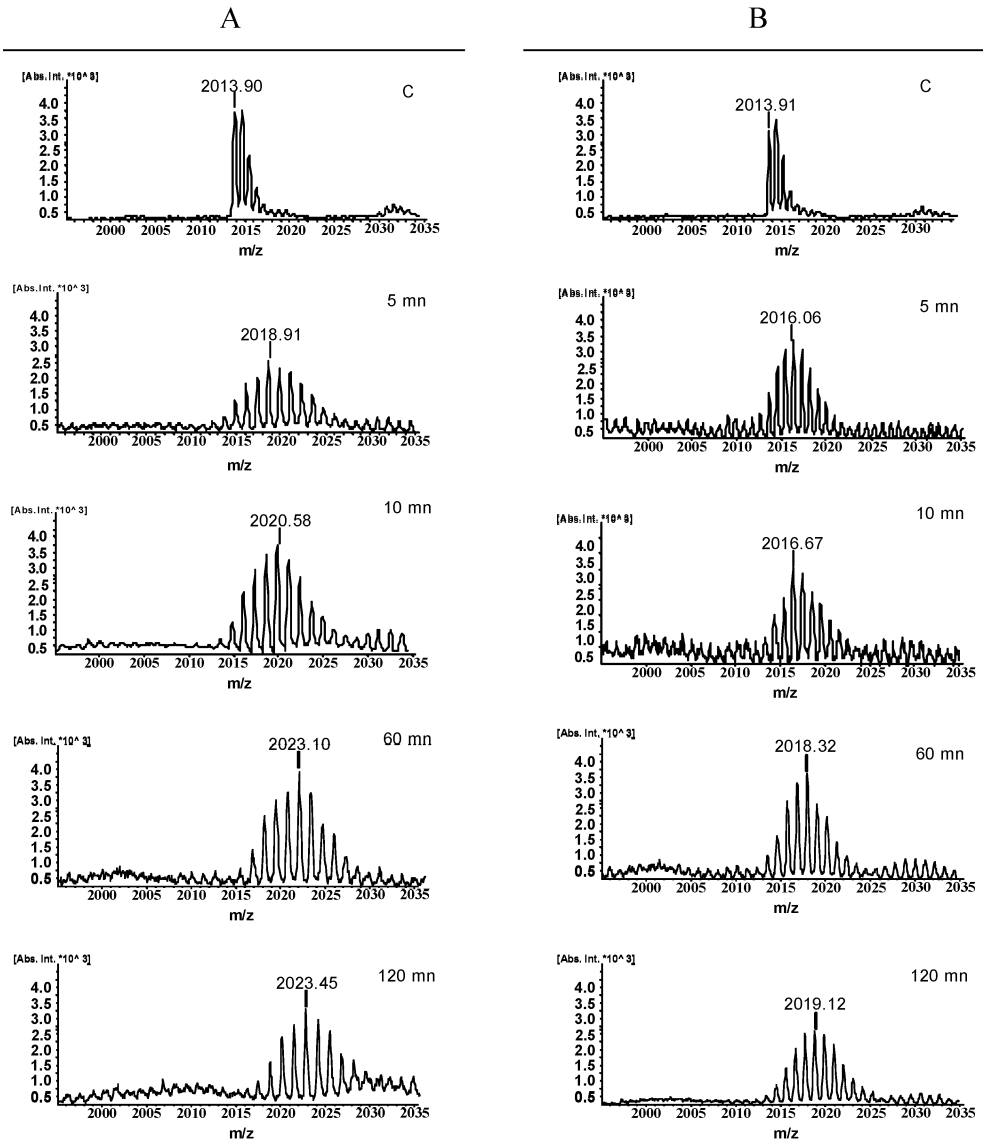

FIGURE 3: MALDI-TOF mass spectra of the peptide [217−234]. HET-s protein (30 pmol/μL) in soluble form (A) or in agregate form (B) was incubated for various times (from 5 to 120 min). After exchange quenching and pepsin digestion, Ziptip simplification is processed, and the elution fraction is directly spotted on the target before MS analysis. Mass values given for the control experiment (C) corresponds to *m*/*z* of the monoisotopic peak for the peptide [217−234]. Mass values given for exchange experiments correspond to *m*/*z* of the centroid of the envelope mass peaks for $[M + H]^+$ pseudo-molecular ions.

TurboSequest program was used to assign peptide sequences from their fragment ions.

RESULTS

Peptide Mapping of HET-s Protein. HXMS experiments require the determination of the peptide map of the protein of interest to evaluate which part of the protein is most accessible to the solvent (*20*). The lack of specificity of pepsin complicates this task since several isobaric peptide ions may be found in the case of HET-s peptides.

In a first step, the conditions of proteolytic cleavage of the soluble form of HET-s by means of immobilized pepsin were adjusted to obtain a majority of peptides in the 1000−3500 Da mass range. In our conditions, this digest produced 62 peaks upon MALDI-MS analysis. To limit as much as possible selective desorption phenomena associated with MALDI-MS, a microchromatographic step gradient separation was applied (on C18 ZipTips, with three elution steps at 20, 40, and 70% acetonitrile, respectively) (*21*). Altogether, 86 different peaks were observed in the three mass spectra of these fractions. Only eight peaks out of 86 could be assigned unambiguously (by exact mass, with a single peptide match within a 20 ppm range, which corresponds to our confidence limit for MALDI-MS measurements). For the other peaks, two or more primary sequences were possible candidates. Thus, in a second step, post source decay (PSD) experiments were performed and allowed the assignment of four other peptides on the basis of their fragmentation. However, these 12 peaks together represented only 45% of HET-s primary structure. Further mass assignments were then sought by means of LC-MS/MS analysis, using an ion trap mass spectrometer operated in the electrospray mode. In this way, we have determined 14 other peptide stretches, for an overall 87% sequence coverage (Table 1 and Figure 1).

The same pattern of digestion was obtained for both HET-s structural conditions (soluble and amyloid form), but the

Table 2: Exchange Rate Calculation of Protected Hydrogen Atoms[a]

exchange rates of protected hydrogen atoms							
HET-s soluble form				HET-s amyloid form			
		intermediate exchange[c]				intermediate exchange[c]	
mass (MH^+) (theor)[b]	position	k_{ex1}[d] (mn^{-1})	k_{ex2} (mn^{-1})	mass (MH^+) (theor)[b]	position	k_{ex1}[d] (mn^{-1})	k_{ex2} (mn^{-1})
1865.86	281−295	3.8×10^{-2}	5.7×10^{-3}	2376.15	25−43	1.8×10^{-2}	1.3×10^{-3}
1403.58	286−295	3.4×10^{-2}	5.7×10^{-3}	1224.62	146−166	1.7×10^{-2}	1.7×10^{-3}
1256.52	287−295	3.1×10^{-2}	5.3×10^{-3}	1815.09	132−147	1.0×10^{-2}	1.3×10^{-3}
2647.25	274−295	3.0×10^{-2}	4.9×10^{-3}	1055.68	43−51	1.0×10^{-2}	1.3×10^{-3}
3403.85	227−258	2.8×10^{-2}	3.6×10^{-3}	1541.85	173−186	9.3×10^{-3}	1.1×10^{-3}
1283.75	236−247	2.7×10^{-2}	3.6×10^{-3}	1075.62	158−166	7.8×10^{-3}	1.0×10^{-3}
1613.78	251−265	2.7×10^{-2}	3.0×10^{-3}	2241.08	4−25	7.6×10^{-3}	1.1×10^{-3}
1345.71	223−234	2.2×10^{-2}	2.5×10^{-3}	1983.09	88−105	5.8×10^{-3}	9.4×10^{-4}
2014.10	217−234	2.2×10^{-2}	2.1×10^{-3}	1756.92	91−105	5.2×10^{-3}	1.2×10^{-3}
1224.62	146−166	1.8×10^{-2}	1.8×10^{-3}	1144.62	28−37	3.9×10^{-3}	8.4×10^{-4}
2376.15	25−43	1.8×10^{-2}	1.4×10^{-3}	1202.69	133−142	3.9×10^{-3}	9.0×10^{-4}
1815.09	132−147	1.1×10^{-2}	1.3×10^{-3}	2072.20	132−149	3.7×10^{-3}	6.9×10^{-4}
1055.68	43−51	9.9×10^{-3}	1.2×10^{-3}	1741.98	44−58	3.6×10^{-3}	7.7×10^{-4}
1541.85	173−186	9.9×10^{-3}	1.2×10^{-3}	2622.43	111−132	3.5×10^{-3}	7.9×10^{-4}
2241.08	4−25	7.8×10^{-3}	1.1×10^{-3}	1262.56	209−221	3.4×10^{-3}	7.0×10^{-4}
1075.62	158−166	7.5×10^{-3}	1.0×10^{-3}	2277.09	193−216	2.9×10^{-3}	7.0×10^{-4}
2277.09	193−216	7.5×10^{-3}	1.0×10^{-3}	2014.10	217−234	2.8×10^{-3}	7.0×10^{-4}
1329.65	65−76	6.1×10^{-3}	9.7×10^{-4}	1613.78	251−265	2.2×10^{-3}	7.0×10^{-4}
1983.09	88−105	5.8×10^{-3}	9.7×10^{-4}	1256.52	287−295	2.2×10^{-3}	5.7×10^{-4}
1756.92	91−105	5.5×10^{-3}	9.2×10^{-4}	1345.71	223−234	2.2×10^{-3}	6.9×10^{-4}
1202.69	133−142	3.6×10^{-3}	9.1×10^{-4}	2647.25	274−295	2.0×10^{-3}	7.0×10^{-4}
1144.62	28−37	3.6×10^{-3}	8.4×10^{-4}	1403.58	286−295	1.9×10^{-3}	6.3×10^{-4}
2622.43	111−132	3.6×10^{-3}	8.0×10^{-4}	3403.85	227−258	1.9×10^{-3}	6.3×10^{-4}
2072.20	132−149	3.6×10^{-3}	8.0×10^{-4}	1283.75	236−247	1.9×10^{-3}	5.3×10^{-4}
1741.98	44−58	2.8×10^{-3}	7.0×10^{-4}	1865.86	281−295	1.9×10^{-3}	5.3×10^{-4}

[a] Exchange rate calculation of protected hydrogen atoms. For the 26 peptides, covering 87% of the HET-s primary sequence, the exchange rates were determined using a kinetic study from 5 to 120 min. This kinetic study indicates the presence of two populations of protected hydrogens having different exchange rates (k_{ex1} and k_{ex2}) for each peptide. The calculation was realized after the hydrogen exchange on soluble and amyloid forms of HET-s protein. In each row, the peptides were classified from the fastest to the slowest exchange rate. [b] Calculated masses (monoisotopic, MH^+) for identified peptides. [c] Intermediate exchange is defined as between 2 and 1000 min. [d] Rate constant (in min^{-1}) of HET-s peptides. Two populations of hydrogens having different constant rates can be distinguished (k_{ex1} and k_{ex2}).

addition of 4 M urea, well-tolerated by the immobilized protease, was required to obtain reproducible results for the amyloid form (Figure 2).

Back Exchange Control. To conduct HXMS experiments on HET-s, we have evaluated the impact of sample preparation on back exchange. The maximal exchange level was determined for peptides of a HET-s pepsin digest after a 120 min incubation in D_2O (26 peptides were considered). The back exchange varied between 10 and 16%. Because some HET-s peptides are thought to aggregate after a few hours, the maximal deuterium incorporation cannot be determined for very long incubation times.

Hydrogen/Deuterium Exchange on the Soluble Form of HET-s. After variable incubation times in deuterium oxide (from 5 to 120 min) and pepsin proteolysis, all assigned sequence stretches were characterized by MALDI-MS. The average mass used for calculation was determined by integrating the cluster of isotopic peaks (Figure 3). For each peptide, deuterium incorporation was plotted as a function of time, and exchange rates were determined from plots of $\ln(P)$ versus t (eq 2). Two populations of exchangeable hydrogens having different rate constants (k_{ex1} and k_{ex2}) can be distinguished within the envelope time from 5 to 120 min. The different exchange rates were classified from the highest to the lowest (Table 2, HET-s soluble form). The highest exchange rates are found in the C-terminal region from 274 to 295. In this region, four peptides ([281−295], [286−295], [287−295], and [274−295]) have exchange rates between 3×10^{-2} and 3.8×10^{-2} min^{-1} for k_{ex1} and between 4.9×10^{-3} and 5.7×10^{-3} min^{-1} for k_{ex2}. Another group having exchange rates between 2.2×10^{-2} and 2.8×10^{-2} min^{-1} for k_{ex1} and between 2.1×10^{-3} and 3.6×10^{-3} min^{-1} for k_{ex2} is composed of five peptides also located in the C-terminal region ([217−234], [223−234], [251−265], [236−247], and [227−258]). A third group of three peptides ([146−166], [25−43], and [173−186]) has exchange rates between 1.1×10^{-2} and 1.8×10^{-2} min^{-1} for k_{ex1} and between 1.3×10^{-3} and 1.8×10^{-3} min^{-1} for k_{ex2}. For the other fragments, exchange rates range from 1.8×10^{-2} to 2.8×10^{-3} min^{-1} for k_{ex1} and from 1.8×10^{-3} to 7×10^{-4} min^{-1} for k_{ex2}. For these peptides, there is no specific region of HET-s protein corresponding to a cluster of exchange rate values.

The percentage of deuterium incorporation was calculated for each fragment and each incubation time. For the overlapping segments, the deuterium incorporation value was calculated as an average of deuterium incorporation of each peptide involved in the overlap. Three regions can be distinguished (Figure 4). The maximal deuterium incorporation is located in the [221−293] C-terminal part of HET-s and reaches 60−74% after 120 min incubation time. For the same incubation time, a [193−221] intermediate region displays a deuterium incorporation ranging from 35 to 60%. Peptides belonging to the [1−193] region have a lower deuteration level (from 27 to 35%). These results clearly designate the C-terminal domain spanning residues 221−

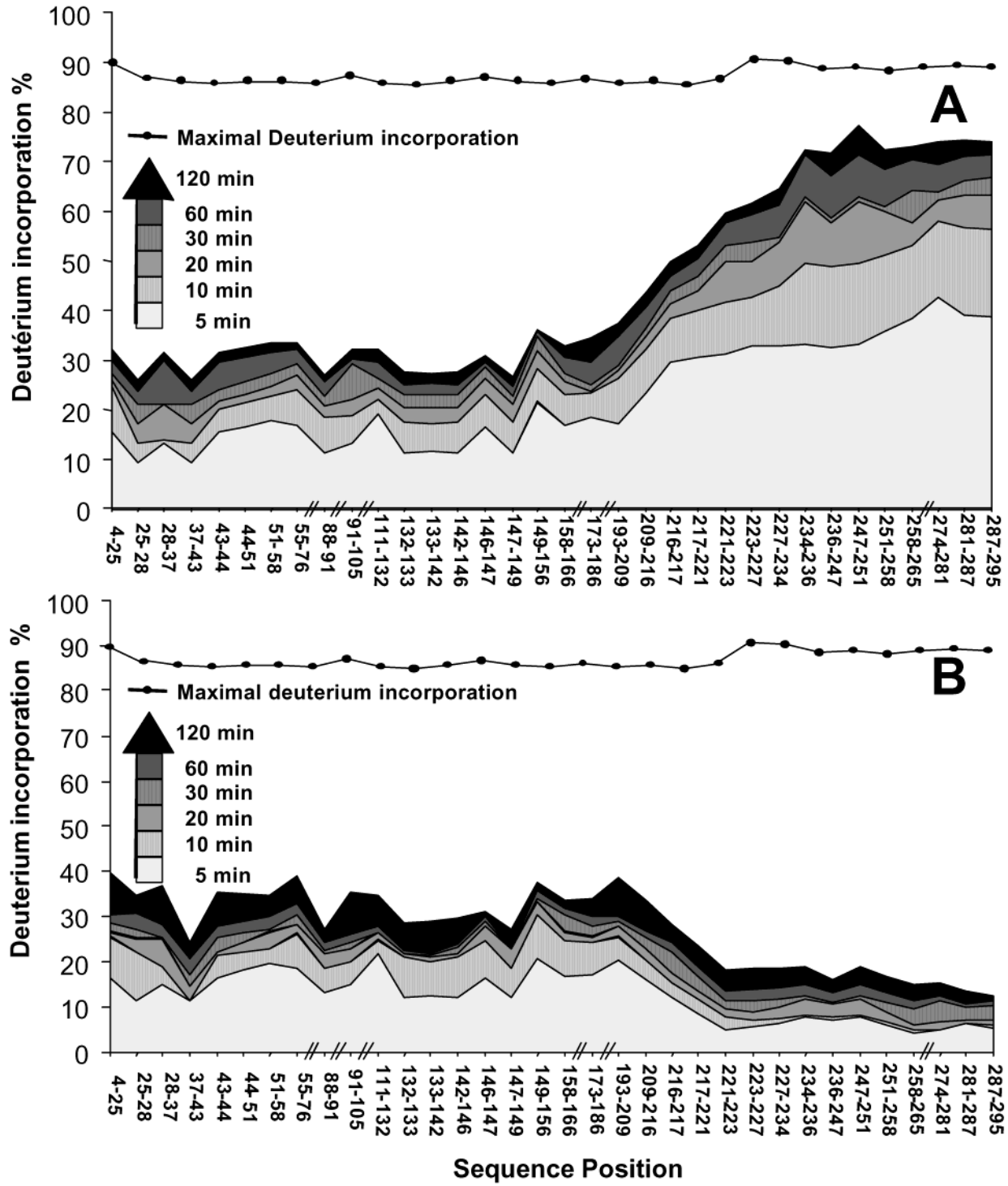

FIGURE 4: HXMS analysis along the sequence of HET-s. (A) A soluble form of HET-s protein was incubated for various time (from 5 to 120 min) in D_2O. After pepsin digestion and MALDI-MS analysis, the exchange level was calculated for each HET-s fragment (as D/H_t where D is the mesured amount of deuterium incorporated, and H_t is the total of exchangeable hydrogens for the fragment). The exchange level of stretches belonging to different peptides was calculated as an average of individual values. (B) An aggregated form of HET-s was analyzed as in panel A. For back exchange control, a pepsin digest of HET-s was incubated for 120 min in D_2O, and after MALDI-MS analysis, the maximal deuterium incorporation was determined for each of these peptides.

295 as the most accessible region of HET-s protein when under its soluble form.

Hydrogen/Deuterium Exchange on Amyloid Form HET-s Protein. Aggregates of HET-s were obtained as previously described (*10*), and amyloid formation was monitored by electron microscopy (Figure 5). When the amyloid form of HET-s protein was incubated in deuterium oxide and subsequently analyzed by MALDI-MS, the lowest exchange levels were evidenced for peptides clustered in the C-terminal region. This cluster is composed of 11 peptides ([281−295], [236−247], [227−258], [286−295], [274−295], [223−234], [287−295], [251−265], [217−234], [193-216], and [209−221]) having exchange rates between 3.4×10^{-3} and 1.9×10^{-3} min^{-1} for k_{ex1} and between 7×10^{-4} and 5.3×10^{-4} min^{-1} for k_{ex2} (Table 2, HET-s amyloid form). The calculation of deuterium incorporation for each peptide of HET-s

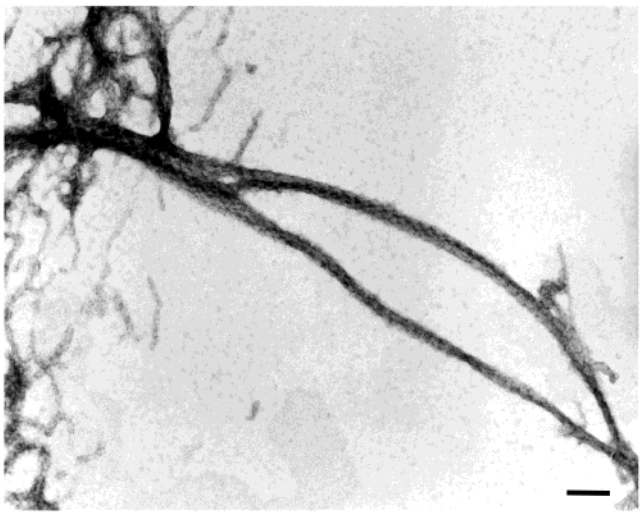

FIGURE 5: Electron microscopy of an aggregated form of HET-s showing amyloid fibrils.

protein revealed that the most protected region is located in the C-terminal region between residues 221 and 295. In this region, the deuterium incorporation reached only 17−20% after 120 min incubation time (Figure 4B). Exchange levels in the N-terminal region of the protein are similar for the soluble and the amyloid form of the protein.

DISCUSSION

Hydrogen exchange can be used to gain insight into the structure and dynamics of proteins. When coupled with mass spectrometry, this method is particularly relevant for the study of amyloid proteins that are otherwise difficult to analyze using other structural biology techniques (*16*, *22*, *23*). Owing to its high speed of analysis, excellent sensitivity, and accuracy, hydrogen exchange coupled to MALDI-MS turns out to be a valuable methodology in structural biology (*24*). The analysis of peptide maps by MALDI-MS after pepsin digestion does not require combined liquid chromatography−mass spectrometry (*15*, *25*). However, in the case of HET-s (289 residues), the mass fingerprint generated by pepsin cleavage was highly complex and required the combined information of MALDI-MS experiments and of electrospray MS/MS analysis to approach 90% sequence coverage. MALDI-MS alone was then used for the rest of the experiments.

Our study indicates that deuterium incorporation is drastically decreased in the C-terminal region of the protein in the amyloid state, while H/D exchange is mostly unchanged in the rest of the protein. Deuterium incorporation drops sharply around residue 217. The [193−216] peptide shows similar exchange levels in both the soluble and the amyloid form, while exchange in the [217−234] peptide is dramatically decreased (Figure 6). Several studies have indicated that the core regions of amyloid aggregates show very limited hydrogen exchange (*16*−*18*). We thus interpret the protection measured in the C-terminal region of HET-s as a consequence of H-bonding in the β-sheet structure of the HET-s amyloid aggregate. This observation indicates that aggregation into a β-sheet rich amyloid structure involves only a limited part of the HET-s protein, namely, the C-terminal region. Delimitation of the amyloid core region of HET-s by our HX experiment is perfectly consistent with the definition obtained by limited proteolysis. The proteinase K resistant core of the HET-s amyloid was found to span residues 218−289 (*12*). This delimitation of the HET-s amyloid core by HXMS constitutes an important confirmation of the results obtained by limited proteolysis. Moreover, HXMS experiments suggest that the level of protection against hydrogen exchange is relatively homogeneous within this C-terminal core region.

The N-terminal region of HET-s forms a globular domain spanning residues 1 to about 230 (*12*). Hydrogen exchange rates measured for most of the peptides corresponding to that region are not drastically modified upon amyloid formation. The Ure2p yeast prion protein also displays a two domain structure with a poorly structured N-terminal prion forming domain and a globular C-terminal domain. It was shown that the globular domain of Ure2p retains its native fold in the fibrils (*26*). Our observation that solvent accessibility in the N-terminal domain of HET-s is almost unmodified upon amyloid formation may suggest that the structure of the globular domain of HET-s is not affected upon aggregation of the C-terminal region. Alternatively, it is conceivable that the structure of the globular domain of HET-s is affected upon aggregation but that the protein retains a substantial amount of secondary structure so that H/D exchange levels are not drastically modified.

The present analysis indicates that in the soluble form of HET-s, a C-terminal region spanning approximately residues 240−289 shows the highest deuterium incorporation and thus displays the highest solvent accessibility. This high solvent accessibility may indicate that this region is highly dynamic and lacks a defined secondary structure. Structural flexibility of that region of HET-s has also been documented using other approaches, including limited proteolysis, NMR, and circular dichroism (*12*). NMR and limited proteolysis experiments gave slightly different results. Limited proteolysis experiments pointed toward an unstructured domain of HET-s starting at residue 240, while NMR suggested that the flexibly disordered region is somewhat longer (*12*). Our HXMS data show that maximal solvent accessibility is reached past residue 240. However, solvent accessibility starts to gradually increase around residue 220. Data from NMR, limited proteolysis, and HXMS studies all indicate that the region past residue 240 is highly flexible. Now, both the limited proteolysis and the HXMS data suggest that the region from residues 220−240 displays an intermediate level of structuration. In other words, it appears that the unstructured domain of HET-s starts at residue 240, while the amyloid core starts at residue 218. Our data thus suggest that the flexible region of HET-s does not overlap completely with the amyloid core.

In summary, this study provides some direct insights into the structural rearrangements occurring upon amyloid aggregation of the HET-s prion protein. We show that modifications in solvent accessibility concern mainly the C-terminal region of the protein. HET-s amyloid formation specifically involves the C-terminal region of the protein, which undergoes a transition from an unstructured to an aggregated state that is highly resistant to hydrogen exchange. Conformational flexibility is thought to be a prerequisite for fibril formation (*3*, *27*). For several amyloid forming proteins, it was shown that fibril formation is linked to destabilization

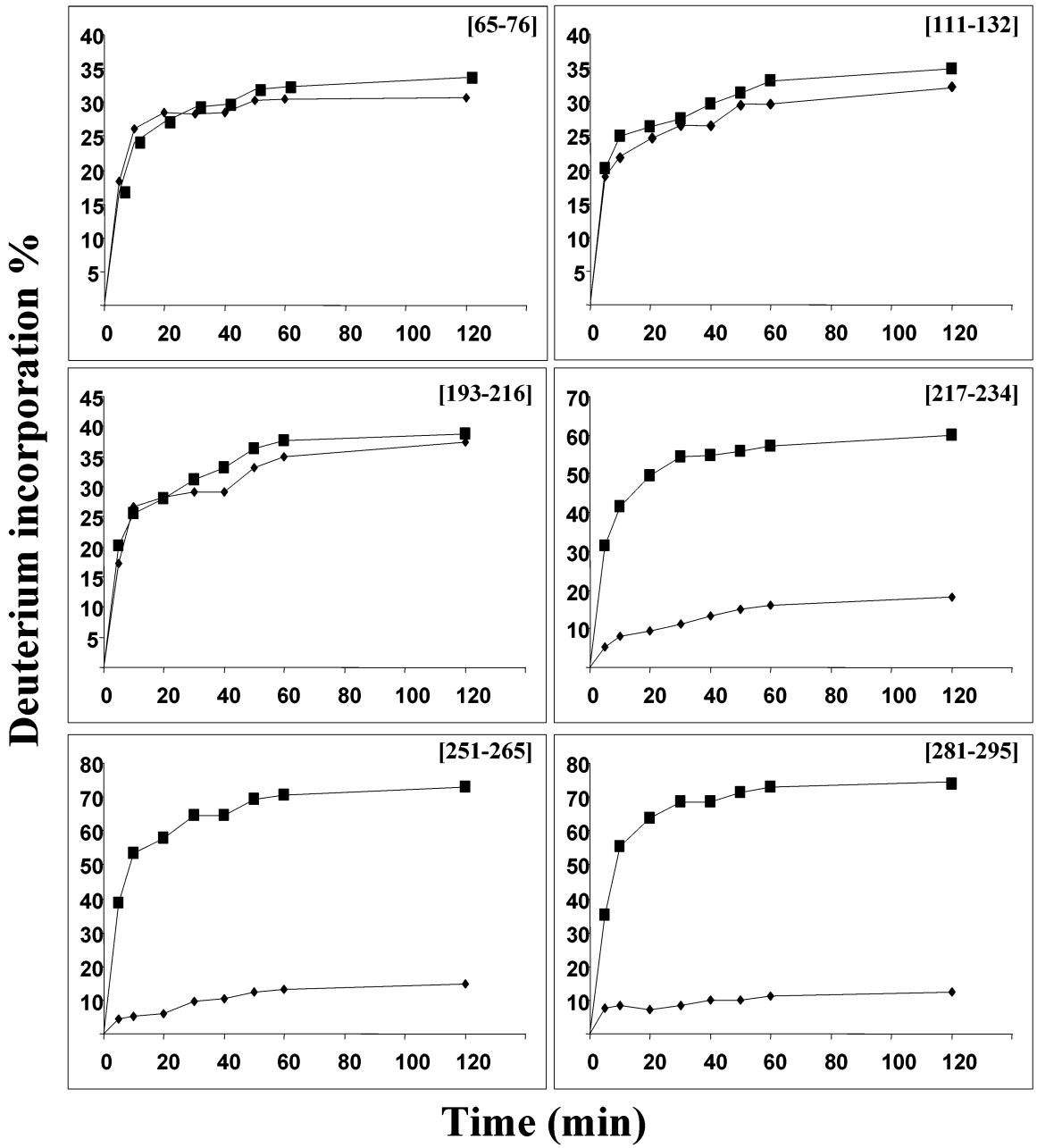

FIGURE 6: Plot of the H/D exchange level (% of D incorporation) as a function of time for HET-s peptides from the soluble (■) and aggregated forms (●). In both cases, HET-s was incubated in D_2O at 25 °C and digested with immobilized pepsin (pH 2, 0 °C, 10 min), and the peptide mixture was separated on a ZipTip and analyzed by MALDI-MS.

of the native state of the protein (*28*−*32*). In particular, it was shown using HXMS that several amyloidogenic proteins show the occurrence of increased conformational dynamics under fibril forming conditions (*22*). Other amyloidogenic proteins such as α-synuclein involved in Parkinson's disease are unstructured in their native state (so-called natively unfolded proteins) (*33*). In the case of HET-s, the C-terminal region appears unstructured in the native form of the protein; thus, fibril formation occurs spontaneously in near physiological conditions and does not require destabilization of the native state of the protein. Like HET-s, the two yeast prion proteins, Sup35 and Ure2p, also display a flexible domain involved in amyloid aggregation attached to a globular domain. This similarity in the overall organization of the fungal prion proteins could suggest that this domain organization is a relevant feature of infectious amyloid proteins.

ACKNOWLEDGMENT

We gratefully acknowledge the help of Prof. Satako Akashi for her contribution to scientific discussions. The authors wish to thank Jacques Shaeffer and Bénédicte Coulary-Salin for the electron microscopy of HET-s fibrils.

REFERENCES

1. Prusiner, S. B. (1998) *Proc. Natl. Acad. Sci. U.S.A. 95*, 13363−83.
2. Koo, E. H., Lansbury, P. T., Jr., and Kelly, J. W. (1999) *Proc. Natl. Acad. Sci. U.S.A. 96*, 9989−90.
3. Rochet, J. C., and Lansbury, P. T., Jr. (2000) *Curr. Opin. Struct. Biol. 10*, 60−8.

4. Wickner, R. B., Edskes, H. K., Maddelein, M. L., Taylor, K. L., and Moriyama, H. (1999) *J. Biol. Chem. 274*, 555−8.
5. Wickner, R. B., Taylor, K. L., Edskes, H. K., Maddelein, M. L., Moriyama, H., and Roberts, B. T. (2000) *J. Struct. Biol. 130*, 310−22.
6. Coustou, V., Deleu, C., Saupe, S., and Begueret, J. (1997) *Proc. Natl. Acad. Sci. U.S.A. 94*, 9773−8.
7. Beisson-Schecroun, J. (1962) *Ann. Genet. 4*, 3−50.
8. Turcq, B., Deleu, C., Denayrolles, M., and Begueret, J. (1991) *Mol. Gen. Genet. 228*, 265−9.
9. Coustou-Linares, V., Maddelein, M. L., Begueret, J., and Saupe, S. J. (2001) *Mol. Microbiol. 42*, 1325−35.
10. Dos Reis, S., Coulary-Salin, B., Forge, V., Lascu, I., Begueret, J., and Saupe, S. J. (2002) *J. Biol. Chem. 277*, 5703−6.
11. Maddelein, M. L., Dos Reis, S., Duvezin-Caubet, S., Coulary-Salin, B., and Saupe, S. J. (2002) *Proc. Natl. Acad. Sci. U.S.A. 99*, 7402−7.
12. Balguerie, A., Dos Reis, S., Ritter, C., Chaignepain, S., Coulary-salin, B., Forge, V., Bathany, K., Lascu, I., Schmitter, J. M., Riek, R., and Saupe, S. J. (2003) *EMBO J. 22*, 2071−2081.
13. Hvidt, A. (1966) *Adv. Protein Chem. 21*, 287−385.
14. Woodward, C. K. (1994) *Curr. Opin. Struct. Biol. 4*, 112−6.
15. Mandell, J. G., Falick, A. M., and Komives, E. A. (1998) *Anal. Chem. 70*, 3987−95.
16. Kheterpal, I., Zhou, S., Cook, K., and Wetzel, R. (2000) *Proc. Natl. Acad. Sci. U.S.A. 97*(*25*), 13597−601.
17. Hoshino, M., Katou, H., Hagihara, Y., Hasegawa, K., Naiki, H., and Goto, Y. (2002) *Nat. Struct. Biol. 9*, 332−6.
18. Kraus, M., Bienert, M., and Eberhard, K. (2003) *Rapid Commun. Mass Spectrom. 17*, 222−8.
19. Liu, Y., and Smith, D. L. (1994) *J. Am. Soc. Mass Spectrom. 5*, 19−28.
20. Juhasz, P., and Martin, S. A. (1997) *Int. J. Mass Spectrom. Ion Proc. 169*, 217−30.
21. Belghazi, M., Bathany, K., Hountondji, C., Grandier-Vazeille, X., Manon, S., and Schmitter, J. M. (2001) *Proteomics 1*, 946−54.
22. Nettleton, E. J., and Robinson, C. V. (1999) *Methods. Enzymol. 309*, 633−46.
23. Kraus, M., Bienert, M., and Krause, E. (2003) *Rapid Commun. Mass Spectrom. 17*, 222−8.
24. Nazabal, A., Vaillier, J., Chaignepain, S., Laguerre, M., Velours, J., and Schmitter, J. M. (2003) *J. Am. Soc. Mass Spectrom. 14*, 471−481.
25. Figueroa, I. D., and Russell, D. H. (1999) *J. Am. Soc. Mass Spectrom. 10*, 719−31.
26. Bousset, L., Thomson, N. H., Radford, S. E., and Melki, R. (2002) *EMBO J. 21*, 2903−11.
27. Dobson, C. M. (1999) *Trends. Biochem. Sci. 24*, 329−32.
28. Booth, D. R., Sunde, M., Bellotti, V., Robinson, C. V., Hutchinson, W. L., Fraser, P. E., Hawkins, P. N., Dobson, C. M., Radford, S. E., Blake, C. C., and Pepys, M. B. (1997) *Nature 385*, 787−93.
29. Chiti, F., Taddei, N., Stefani, M., Dobson, C. M., and Ramponi, G. (2001) *Protein Sci. 10*, 879−86.
30. Dobson, C. M. (2001) *Biochem. Soc. Symp.*, 1−26.
31. Fandrich, M., Fletcher, M. A., and Dobson, C. M. (2001) *Nature 410*, 165−166.
32. Chiti, F., Calamai, M., Taddei, N., Stefani, M., Ramponi, G., and Dobson, C. M. (2002) *Proc. Natl. Acad. Sci. U.S.A. 99 Suppl. 4*, 16419−26.
33. Weinreb, P. H., Zhen, W., Poon, A. W., Conway, K. A., and Lansbury, P. T., Jr. (1996) *Biochemistry 35*, 13709−15.

BI0344275